Microscopic description of $\alpha + N$ bremsstrahlung by a Siegert approach

J. Dohet-Eraly*

Physique Quantique, C. P. 165/82, Physique Nucléaire Théorique et Physique Mathématique, C.P. 229, Université Libre de Bruxelles (ULB), B-1050 Brussels, Belgium and TRIUMF, 4004 Wesbrook Mall, Vancouver, British Columbia V6T 2A3, Canada

(Received 25 November 2013; published 28 February 2014)

A microscopic cluster model of the nucleus-nucleus bremsstrahlung based on an extension of the Siegert theorem, i.e., based on the charge density rather than on the current, allows including implicitly a part of the effects of meson-exchange currents. This approach was developed in a previous paper for zero-spin nuclei and applied to the $\alpha + \alpha$ bremsstrahlung. This model is extended to colliding nuclei with nonzero spins and applied to the $\alpha + p$ and $\alpha + n$ bremsstrahlungs. A comparison between the bremsstrahlung cross sections for these mirror systems is made. The importance of the meson-exchange currents on the $\alpha + N$ bremsstrahlungs is discussed by comparing the $E1$ and $E2$ components of the bremsstrahlung cross sections obtained in the Siegert approach where these currents are partly included and in the non-Siegert approach where they are fully neglected.

DOI: 10.1103/PhysRevC.89.024617 PACS number(s): 25.20.Lj, 24.30.−v, 21.60.Gx, 25.55.−e

I. INTRODUCTION

Nucleus-nucleus bremsstrahlung is a radiative transition between continuum states, where the photon emission is induced by a collision between two nuclei or a nucleus and a neutron. It is an interesting tool for studying the cluster structure of the unbound states [1,2]. It is also interesting by itself, particularly since the perspective of using the $t(d,n\gamma)\alpha$ bremsstrahlung to diagnose plasmas in fusion experiments [3].

The description of electromagnetic transitions in nuclear systems is based on the interaction between the nuclear current and the electromagnetic field of the photon. The nuclear current is caused by the motion of the nucleons and also by the motion of the mesons which are responsible for the nucleon-nucleon (NN) interaction. In most previous studies of nucleus-nucleus bremsstrahlung [4–13], the contribution of the meson-exchange currents is merely neglected. Recently, in Ref. [14], it was proposed to include partially the meson-exchange currents in the bremsstrahlung models by using an extended version of the Siegert theorem [15]. Contrary to the usual Siegert theorem, the extended one [15] does not rely on the long-wavelength approximation, which cannot be used for bremsstrahlung. Indeed, for transitions in the continuum, the initial and final states are not square-integrable and consequently, making the long-wavelength approximation leads to divergent matrix elements of the electric transition multipole operators.

Based on this extension of the Siegert theorem, a microscopic cluster model of bremsstrahlung partially including the meson-exchange currents was developed in Ref. [14] and applied to the $\alpha + \alpha$ system. In this microscopic cluster model, each nucleon of the studied system is taken into account and the scattering wave functions are fully antisymmetrized to satisfy the Pauli principle. The internal wave functions of the colliding nuclei are assumed to have a simple cluster structure in the harmonic-oscillator shell model. The results are derived from an effective NN interaction with one parameter fitted to elastic data only. This microscopic cluster model of bremsstrahlung is extended here to colliding nuclei with nonzero spins and applied to the $\alpha + N$ bremsstrahlungs.

Studying the $\alpha + N$ bremsstrahlungs presents several interests. On the one hand, it makes possible a direct comparison between theory and experiment since the $\alpha + p$ system is one of a few light-ion systems for which experimental bremsstrahlung cross sections exist [16]. On the other hand, the $\alpha + n$ bremsstrahlung has not been studied yet neither experimentally because measurements would be extremely difficult to perform, nor theoretically. The comparison with the mirror reaction of the cross section and of the roles of their $E1$ and $E2$ components is however interesting. Moreover, since it describes the final channel, it is a necessary preliminary step to the more important study of the $t(d,n\gamma)\alpha$ bremsstrahlung.

In Sec. II, the microscopic cluster model of bremsstrahlung is presented and the calculation of the electric transition matrix elements is outlined. The model is applied to the $\alpha + N$ systems in Sec. III for an effective NN interaction adapted to the cluster approach. Contributions of the $E1$ and $E2$ transitions to the bremsstrahlung cross sections are evaluated and a comparison between the $\alpha + n$ and $\alpha + p$ systems is done. The effects of the meson-exchange currents on the $\alpha + N$ bremsstrahlungs are analyzed by comparing the non-Siegert and Siegert cross sections. For the $\alpha + p$ bremsstrahlung, the non-Siegert and Siegert cross sections are also compared with experimental data [16]. Concluding remarks are presented in Sec. IV.

II. NUCLEUS-NUCLEUS BREMSSTRAHLUNG MODEL

A. Cross sections

Two nuclei with reduced mass μ_M collide at the initial relative momentum $\mathbf{p}_i = \hbar\mathbf{k}_i$ in the z direction and relative energy $E_i = p_i^2/2\mu_M$. Each nucleus is characterized by its

*jdoheter@triumf.ca

number of nucleons A_k, its charge $Z_k e$, its parity π_k, its spin I_k, and its spin projection ν_k^i where $k = 1$ or 2. After emission of a photon with energy $E_\gamma = \hbar k_\gamma c$ and momentum $\mathbf{p}_\gamma = \hbar \mathbf{k}_\gamma$ in the direction $\Omega_\gamma = (\theta_\gamma, \varphi_\gamma)$, the system has a final relative momentum $\mathbf{p}_f = \hbar \mathbf{k}_f$ in the direction $\Omega_f = (\theta_f, \varphi_f)$ and a relative energy $E_f = p_f^2/2\mu_M$, which satisfies

$$E_f = E_i - E_\gamma, \tag{1}$$

where the small recoil energy is neglected. The nuclei are assumed to be the same in the initial and final states but for their spin projections, denoted by ν_1^f and ν_2^f after collision. More general formulas, for which this assumption is not done, can be found in Ref. [17].

The bremsstrahlung cross sections are evaluated from the multipole matrix elements, which are proportional to the matrix elements of the electromagnetic transition multipole operators $\mathcal{M}_{\lambda\mu}^\sigma$ between the incoming initial state $\Psi_i^{\nu_1^i \nu_2^i +}$ in the z direction with energy E_i and the outgoing final state $\Psi_f^{\nu_1^f \nu_2^f -}(\Omega_f)$ with energy E_f and direction Ω_f,

$$u_{\lambda\mu}^{\sigma \nu_{12}^{if}}(\Omega_f) = \alpha_\lambda^\sigma \left\langle \Psi_f^{\nu_1^f \nu_2^f -}(\Omega_f) \middle| \mathcal{M}_{\lambda\mu}^\sigma \middle| \Psi_i^{\nu_1^i \nu_2^i +} \right\rangle, \tag{2}$$

where $\sigma = 0$ or E corresponds to an electric multipole and $\sigma = 1$ or M corresponds to a magnetic multipole, ν_{12}^{if} is a shorthand notation for $\nu_1^i \nu_2^i \nu_1^f \nu_2^f$, and α_λ^σ is given by

$$\alpha_\lambda^\sigma = -\frac{\sqrt{2\pi(\lambda+1)} i^{\lambda+\sigma} k_\gamma^\lambda}{\sqrt{\lambda(2\lambda+1)}(2\lambda-1)!!}. \tag{3}$$

Assuming that the photon helicity and the final spin projections are not observed, i.e., the collisions are counted whatever the photon helicity or the final spin projections, and assuming that the incident beam is unpolarized, the differential bremsstrahlung cross section is given by [17]

$$\begin{aligned}\frac{d\sigma}{dE_\gamma d\Omega_\gamma d\Omega_f} = {} & \frac{E_\gamma}{8(\pi\hbar)^4 \hbar c} \frac{p_f^2}{4\pi\epsilon_0 (2I_1+1)(2I_2+1)} \\ & \times \sum_{\nu_{12}^{if}} \sum_{\sigma\sigma'} \sum_{\lambda\lambda'} (-1)^{\lambda+\lambda'+\sigma+\sigma'+1} \\ & \times \sum_{\mu\mu'} (-1)^\mu e^{i(\mu-\mu')\varphi_f} u_{\lambda\mu}^{\sigma \nu_{12}^{if}}(\theta_f, 0) \\ & \times u_{\lambda'\mu'}^{\sigma' \nu_{12}^{if} *}(\theta_f, 0) F_{\mu\mu'}^{\lambda\lambda'\sigma+\sigma'}(\Omega_\gamma),\end{aligned} \tag{4}$$

where

$$\begin{aligned}F_{\mu\mu'}^{\lambda\lambda'\epsilon}(\Omega_\gamma) = {} & \sqrt{4\pi} \sum_j{}' (2j+1)^{-1/2} (\lambda\lambda' \mu -\mu' | j \mu -\mu') \\ & \times (\lambda\lambda' 1 -1 | j 0) Y_j^{\mu'-\mu}(\Omega_\gamma).\end{aligned} \tag{5}$$

The prime on the summation symbol indicates that the sum is restricted to values of j for which $j + \lambda + \lambda' + \epsilon$ is even. Other differential bremsstrahlung cross sections can be obtained by integration. For instance, the angle-integrated cross section is given by

$$\frac{d\sigma}{dE_\gamma} = \frac{1}{1+\delta_{12}} \int \frac{d\sigma}{dE_\gamma d\Omega_f d\Omega_\gamma} d\Omega_f d\Omega_\gamma \tag{6}$$

$$= \frac{E_\gamma}{\pi^2 \hbar^5 c 4\pi\epsilon_0} \frac{p_f^2}{(1+\delta_{12})(2I_1+1)(2I_2+1)} \times \sum_{\nu_{12}^{if}} \sum_{\sigma\lambda\mu} \int_0^\pi \frac{\left| u_{\lambda\mu}^{\sigma \nu_{12}^{if}}(\theta_f, 0) \right|^2}{2\lambda+1} \sin\theta_f d\theta_f, \tag{7}$$

where δ_{12} is equal to unity if nuclei 1 and 2 are identical and to zero otherwise. Dividing by $(1 + \delta_{12})$ is required to take the symmetry of the output channel into account [18].

Experimental differential bremsstrahlung cross sections are measured in the equal-angle coplanar Harvard geometry [16]. For this geometry, nuclei 1 and 2 are detected, respectively, in directions $\Omega_1 = (\theta_1, 0)$ and $\Omega_2 = (\theta_2, \pi)$ and the photon is undetected. Before the collision, nucleus 1 has momentum p_{i1} and nucleus 2 is assumed to be at rest. The bremsstrahlung cross section corresponding to this configuration is given by [17]

$$\begin{aligned}\frac{d\sigma}{d\Omega_1 d\Omega_2} = {} & \frac{k_f p_{i1}^4}{4(\pi\hbar)^4 \mu_M} \frac{\sin^2\theta_1 \sin^2\theta_2}{\sin^5(\theta_1+\theta_2)} \frac{1}{4\pi\epsilon_0 (2I_1+1)(2I_2+1)} \\ & \times \sum_{\nu_{12}^{if}} \sum_{\sigma\sigma'} \sum_{\lambda\lambda'}{}' \sum_{\mu\mu'}{}' (-1)^{\mu+1} u_{\lambda\mu}^{\sigma \nu_{12}^{if}}(\Omega_f) u_{\lambda'\mu'}^{\sigma' \nu_{12}^{if} *}(\Omega_f) \\ & \times \int_0^\pi F_{\mu\mu'}^{\lambda\lambda'\sigma+\sigma'}(\theta_\gamma, 0) d\theta_\gamma.\end{aligned} \tag{8}$$

The prime on the summation symbols indicates that the sums are restricted to the terms such that $\mu + \mu'$ and $\lambda + \lambda' + \sigma + \sigma'$ are even.

The matrix element $u_{\lambda\mu}^{\sigma \nu_{12}^{if}}$ is evaluated by expanding the initial and final states $\Psi_i^{\nu_1^i \nu_2^i +}$ and $\Psi_f^{\nu_1^f \nu_2^f -}(\Omega_f)$ in partial waves. In the microscopic cluster approach presented here, these partial waves are described by the resonating-group method (RGM) [19,20] as

$$\begin{aligned}\Psi_{l_0 I_0}^{JM\pi}(E) = {} & \sqrt{\frac{A!}{A_1! A_2! (1+\delta_{A_1 A_2})}} \\ & \times \sum_{lI} \mathcal{A}\left[Y_l(\Omega_\rho) \left[\phi_{I_1}^{\pi_1} \phi_{I_2}^{\pi_2} \right]^I \right]^{JM} g_{lI,l_0 I_0}^{J\pi}(E, \rho),\end{aligned} \tag{9}$$

where E is the relative energy between the clusters, $A = A_1 + A_2$ is the total number of nucleons in the system, J is the total angular momentum, M is its projection, π is the total parity, l is the relative orbital angular momentum, I is the channel spin, $\phi_{I_1}^{\pi_1}$ and $\phi_{I_2}^{\pi_2}$ are the internal wave functions of the clusters, $\boldsymbol{\rho} = (\rho, \Omega_\rho)$ is the relative coordinate between the cluster centers of mass, $g_{lI,l_0 I_0}^{J\pi}$ is the relative wave function. Indices l_0 and I_0 correspond to the entrance channel. The total parity π is linked with the individual nuclei parities by

$$\pi = \pi_1 \pi_2 (-1)^l. \tag{10}$$

The internal wave functions $\phi^{\pi_1}_{I_1}$ and $\phi^{\pi_2}_{I_2}$ are obtained by removing a c.m. factor from Slater determinants describing the ground states of the clusters within the harmonic oscillator shell model. The normalization of the relative wave function $g^{J\pi}_{lI,l_0I_0}$ is fixed by its asymptotic behavior,

$$g^{J\pi}_{lI,l_0I_0}(E,\rho) \underset{\rho\to\infty}{\longrightarrow} \frac{\sqrt{\pi(1+\delta_{12})(2l_0+1)}i^{l+1}e^{i\sigma_{l_0}(E)}}{\sqrt{v}k\rho}\left[\delta_{ll_0}\delta_{II_0}I_l(\eta,k\rho) - U^{J\pi}_{lIl_0I_0}(E)O_l(\eta,k\rho)\right], \tag{11}$$

where $k=\sqrt{2\mu_M E}/\hbar$ is the wave number, $v=\hbar k/\mu_M$ is the relative velocity, $\eta = Z_1Z_2e^2/4\pi\epsilon_0\hbar v$ is the Sommerfeld parameter, σ_{l_0} is the Coulomb phase shift, $U^{J\pi}_{lIl_0I_0}$ is an element of the unitary and symmetric collision matrix $U^{J\pi}$, and I_l and O_l are the incoming and outgoing Coulomb wave functions.

From the partial waves defined by Eq. (9), the multipole matrix elements can be written as [17]

$$u^{\sigma\nu^{if}_{12}}_{\lambda\mu}(\Omega_f) = 2\sqrt{\pi}\alpha^{\sigma}_{\lambda}\sum_{J_iJ_f}\sum_{l_iI_i}\sum_{l_fI_f}\sum_{lI}\sum_{\nu_i\nu_f}\sum_{M_fm_f}\left(I_1I_2\nu^i_1\nu^i_2|I_i\nu_i\right)\left(I_1I_2\nu^f_1\nu^f_2|I_f\nu_f\right)(l_iI_i0\nu_i|J_i\nu_i)(l_fI_fm_f\nu_f|J_fM_f)(J_i\lambda\nu_i\mu|J_fM_f)$$
$$\times[(2J_f+1)(2l+1)]^{-1/2}Y^{m_f}_{l_f}(\Omega_f)U^{J_f\pi_f}_{lIl_fI_f}(E_f)e^{i[\sigma_{l_f}(E_f)+\sigma_l(E_f)]}\left\langle\Psi^{J_f\pi_f}_{lI}(E_f)\right||\mathcal{M}^{\sigma}_{\lambda}|\left|\Psi^{J_i\pi_i}_{l_iI_i}(E_i)\right\rangle. \tag{12}$$

The convention adopted here to define the reduced matrix element is the same as in Ref. [21]. The sums over ν_i ν_f, M_f, and m_f are only apparent since the Clebsch-Gordan coefficients imply $\nu_s=\nu^s_1+\nu^s_2$ with $s=i,f$, $M_f=\nu_i+\mu$, and $m_f=M_f-\nu_f$.

For some configurations, a lot of partial waves have to be considered in Eq. (12) to obtain converged results. However, since nuclear effects are restricted to few partial waves, the contribution of the other partial waves with higher orbital momenta can be evaluated accurately in a purely Coulombic pointlike nuclei approach. Then, as explained in Ref. [7], the purely Coulombic contribution can be calculated by summing up analytically the partial wave expansion, avoiding the problem of the slow convergence.

In this work, the scattering wave function is described by the generator coordinate method (GCM) [19,20], which can be seen as a particular form of the RGM. In the GCM, the same oscillator parameter b is used for describing the internal wave function of both clusters and the $g^{J\pi}_{lI,l_0I_0}$ relative function is approximated as a sum of projected Gaussian functions $\Gamma_l(\rho,R_n)$ defined by

$$\Gamma_l(\rho,R_n) = (\mu'_M/\pi b^2)^{3/4}e^{-\mu'_M(\rho^2+R_n^2)/2b^2}i_l(\mu'_M\rho R_n/b^2), \tag{13}$$

where R_n are real parameters called generator coordinates, $\mu'_M=A_1A_2/A$, and i_l is a modified spherical Bessel function of the first kind or spherical Hankel function. With this particular choice of $g^{J\pi}_{lI,l_0I_0}$, the partial waves $\Psi^{JM\pi}_{l_0I_0}$ can be written from Slater determinants, which makes systematic the calculation of matrix elements. However, the projected Gaussian functions fail to reproduce the correct asymptotic behavior of $g^{J\pi}_{lI,l_0I_0}$ given by Eq. (11). This problem is solved by the microscopic R-matrix method (MRM) [22,23]. In this approach, the configuration space is divided at the channel radius a into two regions: an internal region ($\rho<a$) where the partial waves $\Psi^{JM\pi}_{l_0I_0}$ are described by the GCM and an external region ($\rho>a$) where the antisymmetrization between the colliding nuclei is neglected and the radial relative function $g^{J\pi}_{lI,l_0I_0}$ is approximated by its asymptotic behavior.

The collision matrix and the coefficients of the expansion of $g^{J\pi}_{lI,l_0I_0}$ in projected Gaussian functions are obtained by solving a Bloch-Schrödinger equation, based on a microscopic Hamiltonian, associated with the continuity condition between the internal and external parts of $\Psi^{JM\pi}_{l_0I_0}$ at a [22,23]. For a value of a chosen larger than the range of the nuclear forces and of antisymmetrization effects between nucleons belonging to different nuclei, the wave function is insensitive to the specific value of a.

B. Electric multipole operators

Since the electric transitions dominate for light-ion bremsstrahlung at low photon energy, the magnetic transitions are not considered hereafter. In the non-Siegert approach, the electric transition multipole operators are given explicitly by [24]

$$\mathcal{M}^{E}_{\lambda\mu} = \frac{ie(2\lambda+1)!!}{m_Nc(\lambda+1)k^{\lambda+1}_{\gamma}}$$
$$\times\sum_{j=1}^{A}\left[\left(\frac{1}{2}-t_{j3}\right)\boldsymbol{\chi}_{\lambda\mu}(k_\gamma,\mathbf{r})\cdot(\mathbf{p}_j - A^{-1}\mathbf{P}_{\text{c.m.}})\right.$$
$$\left.-\frac{1}{2}k^2_\gamma g_{sj}(\mathbf{r}\times\boldsymbol{\nabla})\phi_{\lambda\mu}(k_\gamma\mathbf{r})\cdot\mathbf{s}_j\right]_{\mathbf{r}=\mathbf{r}_j-\mathbf{R}_{\text{c.m.}}}, \tag{14}$$

where m_N is the nucleon mass, $\mathbf{r}_j$, $\mathbf{p}_j$, $\mathbf{s}_j$, and $\mathbf{t}_j$ are the coordinate, momentum, spin, and isospin of nucleon j, $\mathbf{R}_{\text{c.m.}}$ and $\mathbf{P}_{\text{c.m.}}$ are the c.m. coordinate and momentum, $g_{sj}=(g_n+g_p)/2+t_{j3}(g_n-g_p)$, where g_n and g_p are the neutron and proton gyromagnetic factors, respectively, and

$$\boldsymbol{\chi}_{\lambda\mu}(k,\mathbf{r}) = \left(k^2\mathbf{r}+\boldsymbol{\nabla}\frac{\partial}{\partial r}r\right)\phi_{\lambda\mu}(k\mathbf{r}), \tag{15}$$
$$\phi_{\lambda\mu}(k\mathbf{r}) = j_\lambda(kr)Y_{\lambda\mu}(\Omega), \tag{16}$$

with $\mathbf{r}=(r,\Omega)$.

The Siegert electric transition multipole operators are written explicitly as [14]

$$\mathcal{M}^{E(\mathrm{S})}_{\lambda\mu} = \frac{e(2\lambda+1)!!}{k_\gamma^\lambda}\sum_{j=1}^{A}\left(\frac{1}{2}-t_{j3}\right)\phi_{\lambda\mu}[k_\gamma(\mathbf{r}_j-\mathbf{R}_{\mathrm{c.m.}})] + \frac{ie(2\lambda+1)!!}{2m_N c(\lambda+1)k_\gamma^{\lambda+1}}\sum_{j=1}^{A}\Big\{\left(\frac{1}{2}-t_{j3}\right)[\boldsymbol{\chi}_{\lambda\mu}(k_\gamma,\mathbf{r}) - (\lambda+1)\nabla\phi_{\lambda\mu}(k_\gamma\mathbf{r}),\mathbf{p}_j - A^{-1}\mathbf{P}_{\mathrm{c.m.}}]_+ - k_\gamma^2 g_{sj}(\mathbf{r}\times\nabla)\phi_{\lambda\mu}(k_\gamma\mathbf{r})\cdot\mathbf{s}_j\Big\}_{\mathbf{r}=\mathbf{r}_j-\mathbf{R}_{\mathrm{c.m.}}}, \quad (17)$$

where $[\mathbf{a},\mathbf{b}]_+$ is a shorthand notation for $\mathbf{a}\cdot\mathbf{b}+\mathbf{b}\cdot\mathbf{a}$. The spin-dependent terms of the Siegert and non-Siegert operators are the same.

At the long-wavelength approximation, the electric transition multipole operators are reduced in the non-Siegert approach to

$$\widetilde{\mathcal{M}}^{E}_{\lambda\mu} = \frac{ie}{m_N c k_\gamma}\sum_{j=1}^{A}\left(\frac{1}{2}-t_{j3}\right) \times\left[\nabla r^\lambda Y^\mu_\lambda(\Omega)\right]_{\mathbf{r}=\mathbf{r}_j-\mathbf{R}_{\mathrm{c.m.}}}\cdot(\mathbf{p}_j - A^{-1}\mathbf{P}_{\mathrm{c.m.}}) \quad (18)$$

and in the Siegert approach to

$$\widetilde{\mathcal{M}}^{E(\mathrm{S})}_{\lambda\mu} = e\sum_{j=1}^{A}\left(\frac{1}{2}-t_{j3}\right)\left[r^\lambda Y^\mu_\lambda(\Omega)\right]_{\mathbf{r}=\mathbf{r}_j-\mathbf{R}_{\mathrm{c.m.}}}. \quad (19)$$

C. Matrix elements of electric transition multipole operators

The calculation of the matrix elements of electric transition multipole operators is outlined in this section. Details can be found in Refs. [14,17].

Let me note $\mathcal{M}_\lambda$ for $\mathcal{M}^E_\lambda$ or $\mathcal{M}^{E(\mathrm{S})}_\lambda$. The reduced matrix element of $\mathcal{M}_\lambda$ is approximated with a good accuracy by [4]

$$\left\langle\Psi^{J_f\pi_f}_{l_f I_f}\middle||\mathcal{M}_\lambda||\middle|\Psi^{J_i\pi_i}_{l_i I_i}\right\rangle = \left\langle\Psi^{J_f\pi_f}_{l_f I_f\mathrm{int}}\middle||\widetilde{\mathcal{M}}_\lambda||\middle|\Psi^{J_i\pi_i}_{l_i I_i\mathrm{int}}\right\rangle - \left\langle\Psi^{J_f\pi_f}_{l_f I_f\mathrm{int}}\middle||\widetilde{\mathcal{M}}_\lambda||\middle|\Psi^{J_i\pi_i}_{l_i I_i\mathrm{int}}\right\rangle_{\mathrm{ext}} + \left\langle\Psi^{J_f\pi_f}_{l_f I_f\mathrm{ext}}\middle||\mathcal{M}_\lambda||\middle|\Psi^{J_i\pi_i}_{l_i I_i\mathrm{ext}}\right\rangle_{\mathrm{ext}}, \quad (20)$$

where $\Psi^{J\pi}_{lI\mathrm{int}}$ and $\Psi^{J\pi}_{lI\mathrm{ext}}$ designate, respectively, the internal and external parts of the partial waves. The energy-dependence of the wave functions is dropped to simplify the notations. The first matrix element in the right-hand side (r.h.s.) of Eq. (20) is calculated microscopically over the whole space while the last two are evaluated over the external region, by neglecting the antisymmetrization.

The long-wavelength approximation can be done for the matrix elements between $\Psi^{J_i\pi_i}_{l_i I_i\mathrm{int}}$ and $\Psi^{J_f\pi_f}_{l_f I_f\mathrm{int}}$ without that convergence problems arise since the wave functions in the internal region are square-integrable. This approximation, which is not essential, leads to much simpler matrix elements.

The calculation of the first term of the r.h.s. of Eq. (20) can be performed by working with individual nucleon coordinates [4,25], which makes simpler the treatment of the antisymmetrization.

The calculation of the matrix elements evaluated over the external region in Eq. (20) is simplified by neglecting the antisymmetrization between nuclei, consistently with the R-matrix approach, and by replacing the electric transition multipole operators defined by Eqs. (14) and (17) by their asymptotic forms, which can be found in Ref. [17].

III. APPLICATION TO THE $\alpha + N$ BREMSSTRAHLUNGS

A. Model specifications

$E1$ and $E2$ transitions are taken into account in the evaluation of the bremsstrahlung cross sections. Only the spin-independent part of the electric transition multipole operators are considered here since at low-photon energy, the contribution of the spin-dependent terms is expected to be weak. For an energy range similar to the one considered here, the contribution of the $M1$ transitions is calculated for the $\alpha + p$ system in a microscopic approach in Ref. [6]. It is proved to be negligible. $M1$ transitions are thus not considered here.

The oscillator parameter b is set at 1.36 fm to reproduce the experimental α radius. Ten generator coordinates from 0.4 to 8.5 fm in steps of 0.9 fm are used to describe the wave function in the internal region. The effective NN interaction is the sum of the Minnesota interaction [26] and the Coulomb potential. The exchange parameter u is set at the value 0.96 and the spin-orbit strength S_0 at 35.6 MeV fm^5 for $\alpha + n$ and at 35.5 MeV fm^5 for $\alpha + p$. With these values, this model reproduces the experimental phase shifts with a good accuracy [27]. The matrix elements $u^{Ev^{if}_{12}}_{\lambda\mu}$ are calculated by taking account of the contribution of the nuclear effects for the partial waves with an orbital momentum up to $l_{\max} = 7$. The results are not modified significantly when $l_{\max}$ is increased from 7 to 8.

Two values of the channel radius are considered: $a = 7.6$ fm and $a = 8.5$ fm to check the insensitivity of the results with respect to the value of a. Only the results for $a = 7.6$ fm are displayed in the figures.

B. Cross sections

In Figs. 1 and 2, the respective contributions of the $E1$ and $E2$ transitions to the angle-integrated cross sections $d\sigma/dE_\gamma$, given by Eq. (7), are shown as a function of the initial relative energy E_i for three values of the photon energy: $E_\gamma = 1, 5$, and 9 MeV. The angle-integrated cross sections taking the $E1$ and $E2$ transitions into account are simply obtained by summing both individual contributions.

For the $\alpha + p$ system, the absolute differences between cross sections at the two considered values of the channel radius are smaller than 140 nb/MeV for the $E1$ transitions and 0.6 nb/MeV for the $E2$ transitions. For the $\alpha + n$ system, absolute differences between cross sections at the two

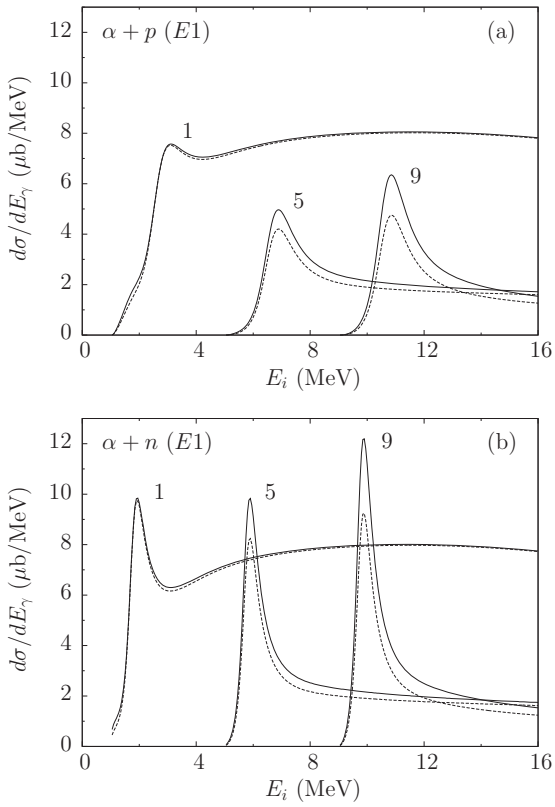

FIG. 1. Contributions of the $E1$ transitions to the angle-integrated cross sections $d\sigma/dE_\gamma$ for $E_\gamma = 1$, 5, and 9 MeV as a function of the initial relative energy E_i for the $\alpha + p$ (a) and $\alpha + n$ (b) systems. Full lines correspond to the Siegert operator $\mathcal{M}^{E(S)}_{\lambda\mu}$ and dashed lines to the non-Siegert operator $\mathcal{M}^{E}_{\lambda\mu}$.

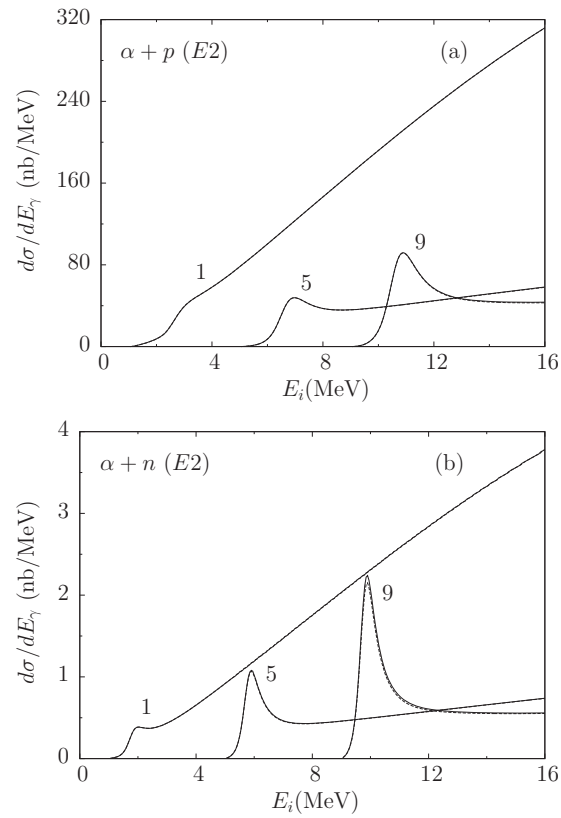

FIG. 2. Contribution of the $E2$ transitions to the angle-integrated cross sections $d\sigma/dE_\gamma$ for E_γ =1, 5, and 9 MeV as a function of the initial energy E_i for the $\alpha + p$ (a) and $\alpha + n$ (b) systems. Notice that scales are very different in both figures. Full lines correspond to the Siegert operator $\mathcal{M}^{E(S)}_{\lambda\mu}$ and dashed lines to the non-Siegert operator $\mathcal{M}^{E}_{\lambda\mu}$. Non-Siegert and Siegert curves are nearly indistinguishable at the scale of the figure.

considered values of the channel radius are smaller than 11 nb/MeV for the $E1$ transitions and 2 pb/MeV for the $E2$ transitions. The differences are often much smaller than these values.

Each cross section shown in Figs. 1 and 2 has a peak at the energy of the final channel corresponding to the $3/2^-$ resonance. Since the $3/2^-$ resonance is at a lower energy for the $\alpha + n$ scattering than for the $\alpha + p$ scattering, the resonances in the bremsstrahlung cross sections are also at a lower energy for the $\alpha + n$ system than for the $\alpha + p$ system. They are thus narrower and more pronounced for the $\alpha + n$ bremsstrahlung than for the $\alpha + p$ bremsstrahlung.

For both systems, the $E1$ transitions largely dominate. The bremsstrahlung cross sections taking the $E1$ and $E2$ transitions into account look thus the same as the contributions of the $E1$ transitions only to the bremsstrahlung cross sections shown in Fig. 1. The contribution of the $E1$ transitions has the same order of magnitude in both systems. Off-resonance, they are even almost identical. On the contrary, the contribution of the $E2$ transitions is about 80 times weaker for the $\alpha + n$ bremsstrahlung than for the $\alpha + p$ one. The ratio of the orders of magnitude of the electric transition contributions can be explained by comparing the effective charges defined by

$$Z^{(\lambda)}_{\rm eff} = Z_1\left(\frac{A_2}{A}\right)^\lambda + Z_2\left(\frac{-A_1}{A}\right)^\lambda. \tag{21}$$

In potential models, where pointlike nuclei are considered, the dominant term of the electric transition multipole operator is proportional to the effective charge at low photon energy as can be proved from relations of Ref. [7]. In first approximation, the ratio between the contributions of a given electric transition for the $\alpha + p$ and $\alpha + n$ bremsstrahlung cross sections is thus given by the square of the ratio between the effective charges

$$\frac{d\sigma(\alpha p, E\lambda)}{d\sigma(\alpha n, E\lambda)} \approx \left(\frac{Z^{(\lambda)}_{{\rm eff},\alpha p}}{Z^{(\lambda)}_{{\rm eff},\alpha n}}\right)^2, \tag{22}$$

where $d\sigma(\alpha N, E\lambda)$ designates the contribution of the $E\lambda$ transitions to the $\alpha + N$ bremsstrahlung cross sections and $Z^{(\lambda)}_{{\rm eff},\alpha N}$ is the effective charge associated with the $\alpha + N$ system. This ratio is equal to 1 for the $E1$ transitions and 81 for the $E2$ transitions.

As noted in the study of the $\alpha + \alpha$ bremsstrahlung [14], the differences between the Siegert and non-Siegert approaches increase with the photon energy. For $E1$ transitions, these differences are nearly negligible at $E_\gamma = 1$ MeV but become quite important beyond $E_\gamma = 5$ MeV. At $E_\gamma = 9$ MeV, for the energy range displayed in Fig. 1, these differences can reach up to around 3.0 μb for the $\alpha + n$ system and up to around

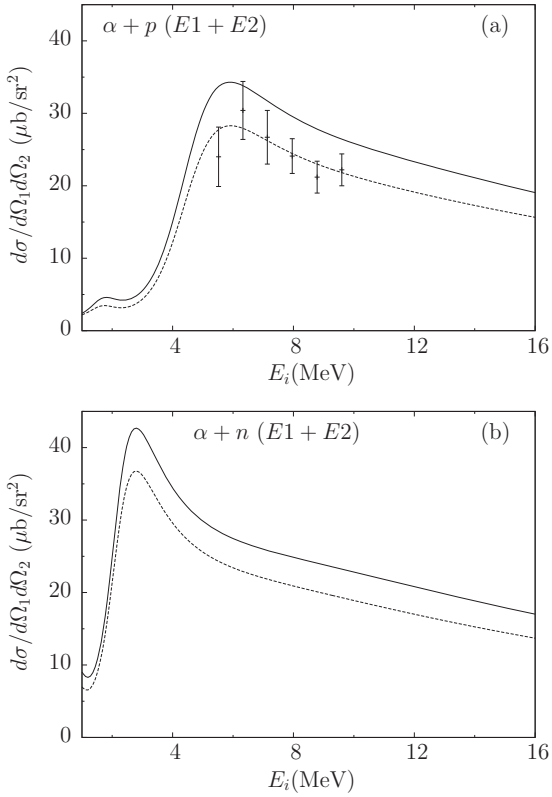

FIG. 3. Laboratory differential cross section $d\sigma/d\Omega_1 d\Omega_2$ in the coplanar geometry at $\theta_N = 70^\circ$ and $\theta_\alpha = 30^\circ$ as a function of the initial energy E_i for $\alpha(p,\alpha p)\gamma$ (a) and $\alpha(n,\alpha n)\gamma$ (b). The $E1$ and $E2$ contributions are taken into account. Full lines correspond to the Siegert operator $\mathcal{M}^{E(S)}_{\lambda\mu}$ and dashed lines to the non-Siegert operator $\mathcal{M}^{E}_{\lambda\mu}$. Experimental data come from Ref. [16].

1.6 μb for the $\alpha + p$ system. For $E2$ transitions, even if the differences between the Siegert and non-Siegert approaches also increase with the photon energy, they are still negligible at $E_\gamma = 9$ MeV. For $E2$ transitions, these differences are much weaker than in the $\alpha + \alpha$ bremsstrahlung. For the three considered photon energies, the Siegert approach leads to higher cross sections than the non-Siegert approach.

Let me compare the model results with experimental data available for the $\alpha(p,\alpha p)\gamma$ bremsstrahlung [16]. The experimental differential bremsstrahlung cross sections are measured in the coplanar Harvard geometry, for which $\theta_p = 70^\circ$ and $\theta_\alpha = 30^\circ$. Differential bremsstrahlung cross sections for this configuration are shown in Fig. 3.

As in Fig. 1, the bremsstrahlung cross sections are higher in the Siegert approach than in the non-Siegert one. The non-Siegert $\alpha + p$ cross section seems to be in a better agreement with the experimental data than the Siegert one. However, the error bars include only statistical errors and are quite important. More numerous and more accurate experimental data are required to perform a conclusive comparison between the Siegert and non-Siegert approaches.

In Fig. 4, the contributions of the $E2$ transitions to the Harvard cross sections are compared for the $\alpha + p$ and $\alpha + n$ systems.

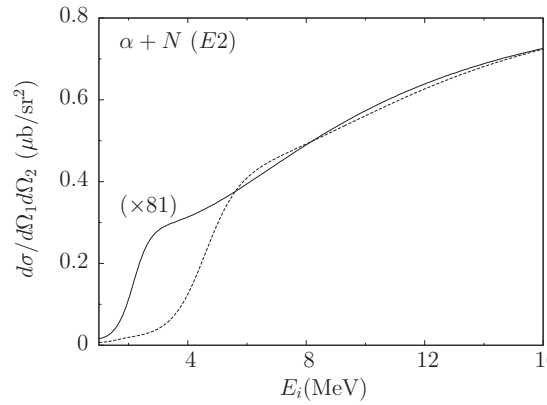

FIG. 4. The $E2$ contributions to the laboratory differential cross section $d\sigma/d\Omega_1 d\Omega_2$ in the coplanar geometry at $\theta_N = 70^\circ$ and $\theta_\alpha = 30^\circ$ as a function of the initial energy E_i for $\alpha(n,\alpha n)\gamma$ (full lines) and $\alpha(p,\alpha p)\gamma$ (dashed lines). The $\alpha + n$ cross sections are multiplied by 81. Siegert and non-Siegert cross sections are indistinguishable at the scale of the figure.

Again, the $E1$ transitions largely dominate and the bremsstrahlung cross sections taking only the $E1$ transitions into account look thus the same as the bremsstrahlung cross sections including the $E1$ and $E2$ contributions, shown in Fig. 3. The contribution of the $E1$ transitions has the same order of magnitude in both $\alpha + N$ systems. Again, differences between the Siegert and non-Siegert approaches are negligible for the $E2$ transitions and the contribution of the $E2$ transitions is about eighty times weaker for the $\alpha + n$ bremsstrahlung than for the $\alpha + p$ bremsstrahlung.

IV. CONCLUSION

A microscopic cluster model of bremsstrahlung, taking implicitly account of a part of the meson-exchange currents by following a Siegert approach, is extended to nonzero spins nuclei and is applied to the $\alpha + N$ systems. It is noted that differences between cross sections obtained with the Siegert and non-Siegert approaches increase with the photon energy and that at a given photon energy, these differences are much larger in the $E1$ transitions than in the $E2$ transitions. In both approaches, for the energies and the configurations that are considered here, the contribution of the $E2$ transitions to the bremsstrahlung cross sections is negligible.

For the $\alpha + p$ bremsstrahlung, the partial inclusion of the meson-exchange currents in the microscopic cluster approach leads to a less good agreement with experiment. The origin of this surprising result merits further investigations as well experimentally as theoretically. Indeed, more numerous and accurate measurements should be useful to know if the Siegert approach deteriorates the agreement with experiment for any configuration or collision energy and if so, to what extent. In a theoretical point of view, a disagreement between the model and the experiment could be due to some simplifying assumptions of the microscopic cluster model as the use of an effective potential to describe the NN interaction or the use of simple cluster wave functions. It should be interesting to verify if this effect is present in *ab initio* bremsstrahlung

calculations based on more realistic NN interactions and more complex wave functions. An *ab initio* model of the $\alpha + N$ bremsstrahlung should be also useful to prepare the *ab initio* study of the $t(d,n\gamma)\alpha$ bremsstrahlung.

The results presented in this paper provide the first theoretical description of the $\alpha + n$ bremsstrahlung. No experimental data are available. The $\alpha + n$ bremsstrahlung cross sections are compared with the $\alpha + p$ ones. The contributions of the $E1$ transitions are very similar for the $\alpha + p$ and $\alpha + n$ systems except for the locations and widths of resonances while the contributions of the $E2$ transitions are very different as expected by a comparison of the effective charges of both systems.

ACKNOWLEDGMENTS

I thank D. Baye for useful discussions and for his comments on the manuscript of this paper. This text presents research results of the interuniversity attraction pole programme P7/12 initiated by the Belgian-state Federal Services for Scientific, Technical and Cultural Affairs. The main part of this work was done with the support of the F.R.S.-FNRS.

[1] V. M. Datar, S. Kumar, D. R. Chakrabarty, V. Nanal, E. T. Mirgule, A. Mitra, and H. H. Oza, Phys. Rev. Lett. **94**, 122502 (2005).
[2] V. M. Datar, D. R. Chakrabarty, S. Kumar, V. Nanal, S. Pastore, R. B. Wiringa, S. P. Behera, A. Chatterjee, D. Jenkins, C. J. Lister, E. T. Mirgule, A. Mitra, R. G. Pillay, K. Ramachandran, O. J. Roberts, P. C. Rout, A. Shrivastava, and P. Sugathan, Phys. Rev. Lett. **111**, 062502 (2013).
[3] T. J. Murphy, C. W. Barnes, R. R. Berggren, P. Bradley, S. E. Caldwell, R. E. Chrien, J. R. Faulkner, P. L. Gobby, N. Hoffman, J. L. Jimerson, K. A. Klare, C. L. Lee, J. M. Mack, G. L. Morgan, J. A. Oertel, F. J. Swenson, P. J. Walsh, R. B. Walton, R. G. Watt, M. D. Wilke, D. C. Wilson, C. S. Young, S. W. Haan, R. A. Lerche, M. J. Moran, T. W. Phillips, T. C. Sangster, R. J. Leeper, C. L. Ruiz, G. W. Cooper, L. Disdier, A. Rouyer, A. Fedotoff, V. Y. Glebov, D. D. Meyerhofer, J. M. Soures, C. Stöckl, J. A. Frenje, D. G. Hicks, C. K. Li, R. D. Petrasso, F. H. Seguin, K. Fletcher, S. Padalino, and R. K. Fisher, Rev. Sci. Instrum. **72**, 773 (2001).
[4] D. Baye and P. Descouvemont, Nucl. Phys. A **443**, 302 (1985).
[5] Q. K. K. Liu, Y. C. Tang, and H. Kanada, Phys. Rev. C **41**, 1401 (1990).
[6] Q. K. K. Liu, Y. C. Tang, and H. Kanada, Phys. Rev. C **42**, 1895 (1990).
[7] D. Baye, C. Sauwens, P. Descouvemont, and S. Keller, Nucl. Phys. A **529**, 467 (1991).
[8] D. Baye, P. Descouvemont, and M. Kruglanski, Nucl. Phys. A **550**, 250 (1992).
[9] Q. K. K. Liu, Y. C. Tang, and H. Kanada, Few-Body Syst. **12**, 175 (1992).
[10] Q. K. K. Liu, Nucl. Phys. A **550**, 263 (1992).
[11] P. Descouvemont and D. Baye, Phys. Lett. B **169**, 143 (1986).
[12] P. Descouvemont, Phys. Lett. B **181**, 199 (1986).
[13] J. Dohet-Eraly, D. Baye, and P. Descouvemont, J. Phys.: Conf. Ser. **436**, 012030 (2013).
[14] J. Dohet-Eraly and D. Baye, Phys. Rev. C **88**, 024602 (2013).
[15] K.-M. Schmitt, P. Wilhelm, H. Arenhövel, A. Cambi, B. Mosconi, and P. Ricci, Phys. Rev. C **41**, 841 (1990).
[16] W. Wölfli, J. Hall, and R. Müller, Phys. Rev. Lett. **27**, 271 (1971).
[17] J. Dohet-Eraly, Ph.D. thesis, Université Libre de Bruxelles (ULB), 2013.
[18] M. L. Goldberger and K. M. Watson, *Collision Theory* (Wiley, New York, 1964).
[19] H. Horiuchi, Prog. Theor. Phys. Suppl. **62**, 90 (1977).
[20] Y. C. Tang, in *Topics in Nuclear Physics II*, Lecture Notes in Physics, Vol. 145, edited by T. T. S. Kuo and S. S. M. Wong (Springer, Berlin, 1981), p. 571.
[21] A. R. Edmonds, *Angular Momentum in Quantum Mechanics* (Princeton University, Princeton, 1957).
[22] D. Baye, P.-H. Heenen, and M. Libert-Heinemann, Nucl. Phys. A **291**, 230 (1977).
[23] P. Descouvemont and D. Baye, Rep. Prog. Phys. **73**, 036301 (2010).
[24] D. Baye, Phys. Rev. C **86**, 034306 (2012).
[25] D. Baye and P. Descouvemont, Nucl. Phys. A **407**, 77 (1983).
[26] D. R. Thompson, M. LeMere, and Y. C. Tang, Nucl. Phys. A **286**, 53 (1977).
[27] R. Kamouni and D. Baye, Nucl. Phys. A **791**, 68 (2007).